

NRC Publications Archive Archives des publications du CNRC

Generation of structured coherent extreme ultraviolet beams from an MgO crystal

Korobenko, A.; Rashid, S.; Heide, C.; Naumov, A. Yu.; Reis, D. A.; Berini, P.; Corkum, P. B.; Vampa, G.

This publication could be one of several versions: author's original, accepted manuscript or the publisher's version. / La version de cette publication peut être l'une des suivantes : la version prépublication de l'auteur, la version acceptée du manuscrit ou la version de l'éditeur.

For the publisher's version, please access the DOI link below. / Pour consulter la version de l'éditeur, utilisez le lien DOI ci-dessous.

Publisher's version / Version de l'éditeur:

<https://doi.org/10.1364/OE.431974>

Optics Express, 29, 15, pp. 24161-24168, 2021

NRC Publications Archive Record / Notice des Archives des publications du CNRC :

<https://nrc-publications.canada.ca/eng/view/object/?id=2eb61cbb-21e1-41f7-b97f-0c681c2beb9c>

<https://publications-cnrc.canada.ca/fra/voir/objet/?id=2eb61cbb-21e1-41f7-b97f-0c681c2beb9c>

Access and use of this website and the material on it are subject to the Terms and Conditions set forth at

<https://nrc-publications.canada.ca/eng/copyright>

READ THESE TERMS AND CONDITIONS CAREFULLY BEFORE USING THIS WEBSITE.

L'accès à ce site Web et l'utilisation de son contenu sont assujettis aux conditions présentées dans le site

<https://publications-cnrc.canada.ca/fra/droits>

LISEZ CES CONDITIONS ATTENTIVEMENT AVANT D'UTILISER CE SITE WEB.

Questions? Contact the NRC Publications Archive team at

PublicationsArchive-ArchivesPublications@nrc-cnrc.gc.ca. If you wish to email the authors directly, please see the first page of the publication for their contact information.

Vous avez des questions? Nous pouvons vous aider. Pour communiquer directement avec un auteur, consultez la première page de la revue dans laquelle son article a été publié afin de trouver ses coordonnées. Si vous n'arrivez pas à les repérer, communiquez avec nous à PublicationsArchive-ArchivesPublications@nrc-cnrc.gc.ca.



Generation of structured coherent extreme ultraviolet beams from an MgO crystal

A. KOROBENKO,¹  S. RASHID,² C. HEIDE,³ A. YU. NAUMOV,¹ D. A. REIS,³ P. BERINI,^{2,4,5}  P. B. CORKUM,¹  AND G. VAMPA^{1,*}

¹Joint Attosecond Science Laboratory, National Research Council of Canada and University of Ottawa, Ottawa, Canada

²Centre for Research in Photonics, University of Ottawa, Ottawa, Canada

³Stanford PULSE Institute, SLAC National Accelerator Laboratory, Menlo Park, California, CA 94025, USA

⁴School of Electrical Engineering and Computer Science, University of Ottawa, Ottawa, Ontario, Canada

⁵Department of Physics, University of Ottawa, Ottawa, Canada

*gvampa@uottawa.ca

Abstract: Short wavelength high-harmonic sources are undergoing intense development for applications in spectroscopy and microscopy. Despite recent progress in peak and average power, spatial control over coherent extreme ultraviolet (XUV) beams remains a formidable challenge due to the lack of suitable optical elements for beam shaping and control. Here we demonstrate a robust and precise approach that structures XUV high-order harmonics in space as they are emitted from a nanostructured MgO crystal. Our demonstration paves the way for bridging the numerous applications of shaped light beams from the visible to the short wavelengths, with potential uses for applications in microscopy and nanoscale machining.

© 2021 Optical Society of America under the terms of the [OSA Open Access Publishing Agreement](#)

1. Introduction

The development of short-wavelength coherent light sources is one of the frontiers of ultrafast science. Impressive technological leaps are being achieved at both large scale facilities, such as X-ray free electron lasers, and in smaller laser laboratories. For example, with free-electron lasers it is now possible to generate X-ray pulses of attosecond duration [1] with unprecedented power and coherently combine multiple Extreme Ultraviolet (XUV) colors [2]. At the laboratory scale, high-harmonic sources can generate soft X-ray photons in the transparency window of water [3–5] ($300 \text{ eV} < h\nu < 500 \text{ eV}$), and high average power XUV sources are being developed thanks to femtosecond Ytterbium pump lasers [6].

Despite these advances, XUV laser beams still lack the degree of control that is routinely achieved with traditional visible and infrared lasers, where spatial, temporal and polarization properties can be tuned with conventional transparent optical materials. *Structured light* has greatly extended the reach of optical lasers, with prominent applications in super-resolution microscopy, optical tweezers, quantum communication (see Ref. [7] for a review). Shaping short-wavelength beams is very challenging due to the strong absorption, especially in the XUV and soft x-ray regime. Producing tailored XUV beams requires a different method.

An effective approach to achieve structured light utilizes the nonlinearity of high-harmonic generation to transfer the properties of the driving infrared laser beam to the generated short-wavelength photons. Therefore, only a precise control of the infrared beam is required - which is easily achieved. For example, polarization-structured infrared fields [8,9] generate circularly-polarized high harmonics - of use for ultrafast magnetization studies [10,11], and vortex infrared beams [12,13] generate XUV photons with orbital angular momentum.

Rather than structuring the driving laser beam, one can pattern the nonlinear medium. This method can be applied to solids, from which high harmonics can be generated [14,15]. In

Ref. [16], ZnO and Si nanocones modify an infrared driver resulting in the generation of high harmonics from a periodic arrangement of localized hotspots. The far-field distribution of the high harmonics encodes the periodic near-field arrangement as a regular diffraction pattern. In the same work, a Fresnel zone plate is fabricated by Ga-ion implantation of the Si surface. High harmonics generated from such surface automatically focus down to the numerical aperture of the zone plate. Recently, Fresnel zone plates milled in a ZnO crystal were utilized to generate focused vortex high harmonics [17]. In Ref. [18,19], plasmonic structures create nanoscale hotspots where high-harmonic emission is preferentially initiated. Waveguides have also been explored as a means to control high-harmonic emission [20]. Finally, enhanced and controlled high-harmonic emission can occur from metasurfaces [21]. With one notable exception [18], all prior work was limited to visible and ultraviolet harmonics.

Here we report a robust method to control the spatial properties of high-harmonic beams at XUV photon energies. To achieve this control we utilize nanostructured MgO crystals, because MgO is known to emit XUV high harmonics [22]. With a nano-fabrication method that we developed, we create micron-scale 1- and 2-dimensional gratings on the surface of MgO with nanometer-scale depth profiles. Just like in ordinary gratings, when an intense infrared laser pulse illuminates the MgO surface it acquires a phase modulation across the beam due to the nanoscale depth of the grooves, while simultaneously generating high harmonics from the grating itself. The harmonics inherit the same phase modulation, multiplied by the harmonic order, and are therefore very efficiently diffracted. We record clear far-field diffraction patterns that demonstrate a highly precise control of the spatial properties of XUV beams emitted from the crystal. Our demonstration paves the way for the generation of more complex XUV structured beams.

The manuscript is structured as follows. In section 2, we present our newly-developed fabrication procedure to produce micro and nano-structures on MgO surfaces. Then, in section 3, we detail the experimental setup for measuring the diffracted high harmonics. Finally, in section 4, we present and discuss the measured diffraction patterns. Finally, we draw the conclusions.

2. Fabrication

Our fabrication method consists of helium-ion beam lithography using polymethylmethacrylate (PMMA) resist as a mask, followed by transfer of the pattern defined in PMMA into the underlying MgO crystal with a wet chemical etch. The process is detailed below.

A (100)-oriented MgO substrate (MTI Corporation) is dehydration-baked at 200 °C on a hot plate for an hour, then exposed to Ar reactive ion etching (RIE, SAMCO 10NR system) for 2 min at an applied RF power of 25 W, Ar flow rate of 10 SCCM and a chamber pressure of 3 Pa to remove surface contaminants. We immediately spin-coat PMMA resist (950k MW, 2% wt. in anisole, Kayaku Advanced Materials) on the MgO substrate to a thickness of 70 nm (Laurell WS-650-23NPP spin coater), then bake the sample at 200 °C for 15 hours. Then, we spin-coat ESPACER 300Z (SHOWA DENKO) on the substrate to dissipate charging during ion beam patterning. We pattern the structures with the helium ion microscope (HIM, Orion NanoFab, Zeiss; Nano Patterning and Visualization Engine, Fibics). A beam current of 1.5 pA at a landing energy of 25 kV is used to deliver a dose of 8 $\mu\text{C}/\text{cm}^2$ with a beam step size of 1 nm, and a dwell time of 0.2 μs . The patterning process of PMMA with a helium ion beam is described elsewhere in detail [23]. Post-exposure, we submerge the substrate in a deionised (DI) water bath for 30 s to remove ESPACER 300Z, rinse it with DI water and dry it with nitrogen. Then, we develop PMMA in a mixture of methyl isobutyl ketone (MIBK):IPA in a ratio of 1:3 for 2 min at 20 °C, followed by a 30 s bath in IPA. A step height of 41 nm is etched into the MgO by submerging the substrate in 25% H_3PO_4 for 43 s at room temperature. Finally, we submerge the substrate in acetone for 2 min to remove PMMA and another 30 s in an IPA bath.

Our fabrication method is born out of our recent development of helium-ion beam lithography on PMMA for plasmonic applications [23], but replacing the liftoff and metal deposition steps

with wet-etch of the MgO substrate. Wet etch of MgO has been demonstrated previously using H_3PO_4 and an SiO_2 mask [24]. We replace the SiO_2 mask with PMMA to make the process compatible with our lithographic approach.

Figures 1(a) and (b) show an AFM scan of the 41 nm-deep etched structures, obtained in tapping mode using a Park Systems NX10 atomic force microscope (AFM) with a Tap300Al-G tip (NanoAndMore). Figure 1(c) shows a HIM image of a 41 nm-deep, $50 \times 50 \mu\text{m}^2$ grating with a $4 \mu\text{m}$ pitch etched in MgO. Figure 1(d) shows a zoomed-in image of the grating and the measured dimensions. Figure 1(e) shows a HIM image acquired at a stage tilt of 54° revealing the RMS roughness, R_q , of the etched MgO and the non-etched surface to be 2.9 nm and 0.8 nm, respectively. We obtain the R_q roughness from the AFM scan shown in Fig. 1(a). Figure 1(f) shows a HIM image of a 33 nm-deep, $50 \times 50 \mu\text{m}^2$ two-dimensional grating with a $4 \mu\text{m}$ pitch etched in MgO, fabricated with a similar procedure. All gratings have a nominal duty cycle of 50%. Deviations from the nominal value, visible in Fig. 1(d) are due to imperfections of the fabrication process. The duty cycle is clearly imprinted on the diffracted high harmonics, as explained below.

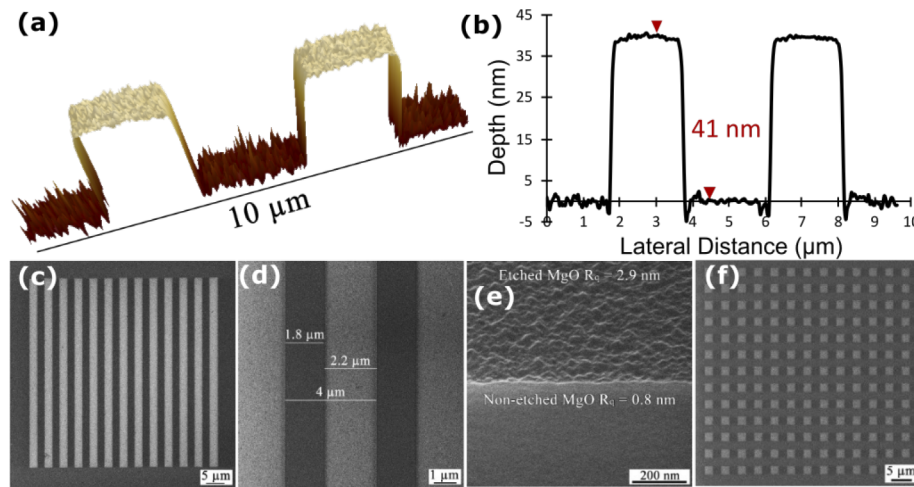


Fig. 1. (a) AFM scan of etched structures in MgO. These structures are transferred from a PMMA pattern through wet etching in 25% H_3PO_4 . (b) Depth profile of the etched structures in MgO gives a step height of 41 nm. (c) HIM image taken with an electron flood gun of a $50 \times 50 \mu\text{m}^2$ grating with a $4 \mu\text{m}$ pitch and $\approx 50\%$ duty cycle etched in MgO and (d) at a high magnification with feature measurements labelled in white. (e) High magnification HIM image acquired at a stage tilt of 54° with R_q roughness of the etched MgO and non-etched MgO surface labeled in white. R_q roughness values were obtained from the AFM scan shown in (a). (f) HIM image of a $50 \times 50 \mu\text{m}^2$ two-dimensional grating with a $4 \mu\text{m}$ pitch, $\approx 50\%$ duty cycle and 33 nm-deep etched in MgO.

3. Experimental setup

After fabrication, the nanostructured crystals are loaded into a vacuum chamber equipped for the generation and detection of the high harmonics. This optical setup is detailed below.

The experimental setup is illustrated in Fig. 2. The fabricated sample is mounted on micro-positioning stages inside a vacuum chamber, which is kept at 2×10^{-6} mbar. We focus infrared laser pulses on the sample, in reflection geometry, with an off-axis parabolic mirror with 25 mm diameter and 25 mm focal length. The pulses are obtained from a Coherent Legend Ti:Sapphire amplifier (800 nm wavelength), with 50 fs duration and repetition rate of 1 kHz. We measure the

generated XUV spot size at the crystal, which is the XUV source, by scanning an edge of the grating structures across the infrared focus. It is $\approx 10 \mu\text{m}$. The peak intensity of the infrared beam on the crystal is estimated to be $10 \text{ TW}/\text{cm}^2$, consistent with previous reports [22,25]. The angle of incidence on the crystal surface is 60° , which corresponds to Brewster angle for 800 nm light. In this geometry, reflection of the infrared beam vanishes for the employed p-polarization, and thus an XUV beam free of infrared contamination is emitted in the direction of specular reflection [26]. The linear laser polarization is parallel to the (100) crystal orientation, which yields the brightest harmonics [22].

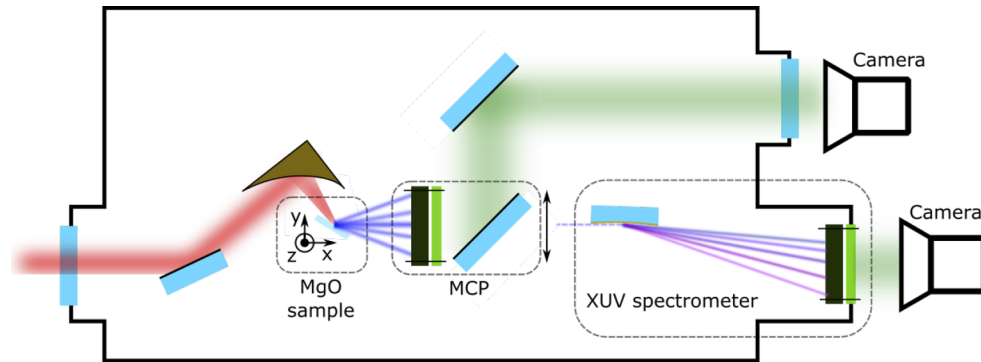


Fig. 2. Sketch of the experimental setup. The driving infrared laser (red line) is focused on the MgO crystal with an angle of incidence of 60° . The vacuum chamber is equipped with a 2"-diameter MCP (dual stack, chevron configuration) and phosphor (P43) detector, mounted on a translation stage that moves transverse to the emitted high-harmonic beam (purple lines). This assembly is positioned within a few cm of the MgO crystal, so to collect high harmonics that diffract with large transverse momentum. Alternatively, this assembly can be translated away to allow the non-diffracted high-harmonic beam to be captured by an XUV spectrometer, consisting of a flat-field grating and a flanged MCP and phosphor assembly. The phosphor screens are imaged with two cameras. The sample is mounted on (x,y,z) micropositioners.

A 2"-diameter microchannel-plate detector (MCP) with a phosphor screen measures the diffracted XUV with $\text{NA} = 0.2$. The phosphor image is relayed outside the vacuum chamber and acquired with a high-speed camera capable of operating at 500 Hz (FLIR Blackfly S). The camera can either integrate over several laser shots, or capture every other laser shot. In the latter case, a separate fast thread thresholds the CMOS image to remove background counts and bins the position of individual photon hits above the threshold. The MCP is operated at saturation to ensure that no information is encoded in the intensity of the hit. Moreover, we ensure that only a few hits per image are recorded to avoid overlapping hits (which would not be counted properly). This "hit count" mode is crucial for the recording of small diffracted signals as it greatly improves the signal-to-noise ratio of the images by removing the dark counts from the CMOS or CCD chip for long exposure times. The MCP can be translated horizontally to acquire a larger momentum space, or to allow the XUV beam to propagate directly into the spectrometer.

Downstream of the MCP is an XUV spectrometer equipped with a flat-field grating (Shimadzu 30-006, 300 l/mm) which resolves the emitted spectrum on a second MCP+phosphor assembly (flanged), when the first MCP is moved out of the XUV beam.

4. High-harmonic measurements

Figure 3 shows diffraction images obtained by illumination of two different gratings, plotted in the reciprocal (momentum) space. We convert the real-space image to reciprocal space, first, by

projecting it on a slanted plane parallel to the crystal surface (that is, a rotation of 60 degrees about the vertical axis) and, second, by transforming the position of each pixel to the parallel momentum $k_{x,y} = 2\pi/\lambda \sin(\theta)$, where λ is the high-harmonic wavelength and θ is the angle of the scattered light with respect to the direction of specular reflection. This procedure is required to account for the slanted positioning of the MCP with respect to the crystal surface.

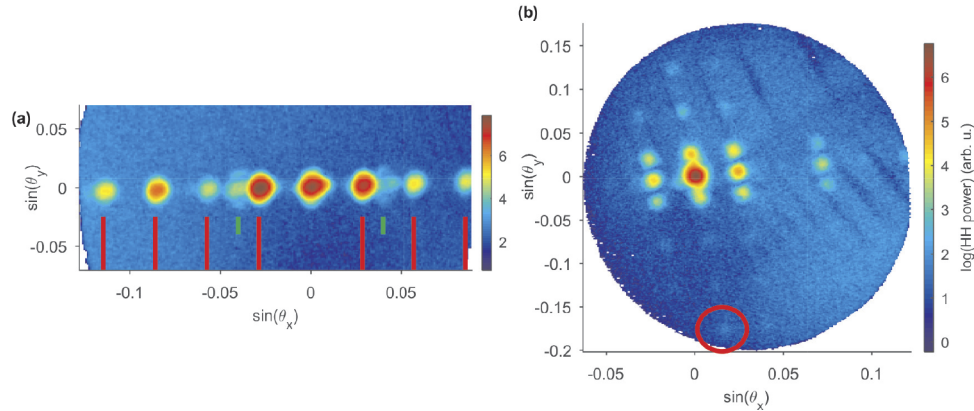


Fig. 3. Diffracted high-harmonic power recorded on the MCP, operated in *hit count* mode, plotted in momentum space, as a function of the sine of the scattering angle: (a) 41 nm-deep wet-etched one-dimensional grating; (b) 33 nm-deep wet-etched two-dimensional grating. The pitch of all gratings is 4 μm . Diffraction orders of harmonics 5 and 7 are marked by the green and red vertical lines in panel (a), respectively. In panel (b), only the 7th harmonic is visible. The circled area marks the 7th diffracted order.

Figures 3(a) and (b) correspond to the 41 nm-deep one-dimensional grating and the 33 nm-deep two-dimensional grating, respectively. Clear diffraction of harmonic 7 is visible in all figures, up to the 4th order in panel (a), red vertical lines, and up to the 7th in panel (b), red circle. Weaker diffraction orders of harmonic 5 are also visible in panel (a) (green lines). Therefore, the structured crystal controls the spatial properties of XUV high harmonics. In agreement with the emitted spectrum measured by the spectrometer, shown in Fig. 4, most of the scattered signal comes from harmonic 7, corresponding to 114 nm wavelength (10.9 eV photons).

The spectral amplitude is seen to vary quite markedly among the various diffracted orders. For example, the odd orders are significantly stronger than the even orders. Furthermore, the 33 nm grating (panel b) completely suppresses the even orders. We expect our flat groove profile to diffract only the odd orders, because this is the harmonic content of a square wave with 50% duty cycle. However, if the duty cycle is different than 50%, even orders can be generated too. Indeed, Fig. 1(d) clearly shows unequal widths for ridges and trenches, and thus explains the detection of even orders in Fig. 3(a).

Given the significant depth of the gratings relative to the harmonic wavelength, the grooves largely act as phase-retarders (a phase grating). Upon illumination of the grating with an angle of incidence of 60°, the infrared driver acquires a phase delay between the grooves and the trenches equal to $\Delta\phi = -4\pi h \cos(\alpha)/\lambda$, where h is the etch depth, α is the angle of incidence, and $\lambda = 800$ nm is the infrared wavelength. The high harmonics inherit this delay, multiplied by the harmonic order. Thus, we expect a delay of 1.3 rad and 1.8 rad for harmonics 5 and 7 on the 33 nm-deep grating, and 1.6 rad and 2.3 rad for the same harmonics on the 41 nm-deep grating. This delay can be controlled with the etch depth and the angle of incidence, and influences the strength of the 0th and the other even orders relative to the odd ones.

Besides the phase modulation, we also measure a slight amplitude modulation between etched and non-etched surfaces. To compare the two surfaces, we measure the undiffracted power from a

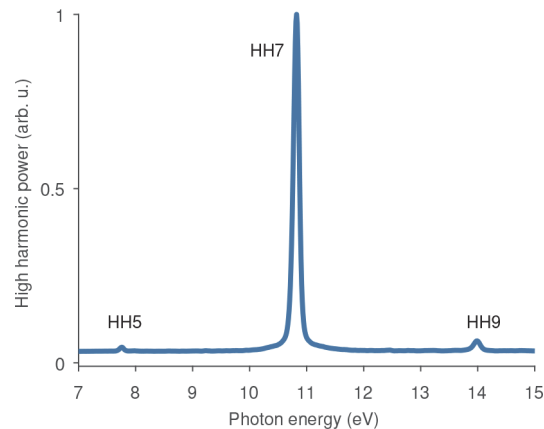


Fig. 4. High-harmonic spectrum generated from the MgO crystal and recorded with the XUV spectrometer. The long (50 fs) driving pulse duration, and the low sensitivity of the MCP below ≈ 10 eV, result in the detection of a nearly monochromatic spectrum at the 7th harmonic.

pristine MgO crystal and from a flat $100 \times 100 \mu\text{m}^2$ etched square. The etched surface yields 14% less high-harmonic power (7% amplitude modulation), possibly due to a chemical change that affects high-harmonic generation or, to a lesser extent, increased surface roughness (as shown in Fig. 1(e)). The diffracted power in Fig. 3 in the first orders (combined) amounts to $\approx 50\%$ of the total power. Thus, we demonstrate efficient control to structure XUV beams.

5. Conclusions

We developed a wet-etch method to fabricate structures on MgO surfaces and we used these structures to control the spatial properties of coherent XUV beams generated thereon. Our results represent a major breakthrough to develop "short-wavelength structured light" and nanofocused XUV beams. The latter can be achieved with patterned Fresnel zone plates [16,17]. Given that MgO is known to be among the most efficient solid-state emitters of high harmonics, we foresee that our solid-state device can be, in the future, utilized for structured illumination in photoelectron imaging experiments [27–29], high-resolution imaging and spectroscopy with elemental and chemical specificity, and nanoscale laser ablation [30,31]. For nanoscale ablation and imaging, we estimate that an intensity on the order of 0.1 TW/cm^2 can be achieved in a nanofocused XUV beam. This estimate is obtained by considering an infrared beam of $\approx 10 \mu\text{m}$ diameter that illuminates a Fresnel zone plate patterned on MgO, which generates an XUV high harmonic with a wavelength of $\approx 100 \text{ nm}$ focused to $\approx 100 \text{ nm}$. This corresponds to a 10^4 reduction of the focal area. Given the measured diffraction efficiency of $\approx 50\%$ in the first orders of diffraction (combined), and assuming a conversion efficiency of 10^{-6} from infrared power to that of one high-order harmonic, we estimate a conversion of infrared to focused XUV intensity of 10^{-2} , which yields 0.1 TW/cm^2 , as stated above. We note that a 3-dimensional control over the grating depth, such as obtained from a blazed etch profile, can achieve measured diffraction efficiencies of 76% [17]. Furthermore, the pulse duration of the high harmonic is likely shorter than the infrared one, and will thus increase the intensity further. Future developments include the extension of the photon energy range employing shorter laser pulses [25].

Funding. Defense Threat Reduction Agency (HDTRA1-19-1-0026); Alexander von Humboldt-Stiftung; W. M. Keck Foundation; Air Force Office of Scientific Research (FA9550-16-1-0109).

Acknowledgments. G. V., C. H. and D. A. R. acknowledge funding from the W. M. Keck foundation. C. H. acknowledges support by the Alexander von Humboldt Foundation. G. V., A. K and P. B. C. acknowledge support

from the Joint Center for Extreme Photonics. P. B. C. acknowledge funds from US Defence Threat Reduction (DTRA) (HDTRA1-19-1-0026) and from US Air Force Office of Scientific Research (AFOSR) (FA9550-16-1-0109). G. V. thanks Dave Crane and Ryan Kroeker for providing precious technical support.

Disclosures. The authors declare no conflicts of interest.

Data availability. Data underlying the results presented in this paper are not publicly available at this time but may be obtained from the authors upon reasonable request.

References

1. J. Duris, S. Li, T. Driver, E. G. Champenois, J. P. MacArthur, A. A. Lutman, Z. Zhang, P. Rosenberger, J. W. Aldrich, R. Coffee, G. Coslovich, F.-J. Decker, J. M. Glowina, G. Hartmann, W. Helml, A. Kamalov, J. Knurr, J. Krzywinski, M.-F. Lin, J. P. Marangos, M. Nantel, A. Natan, J. T. O'Neal, N. Shivaram, P. Walter, A. L. Wang, J. J. Welch, T. J. A. Wolf, J. Z. Xu, M. F. Kling, P. H. Bucksbaum, A. Zholents, Z. Huang, J. P. Cryan, and A. Marinelli, "Tunable isolated attosecond x-ray pulses with gigawatt peak power from a free-electron laser," *Nat. Photonics* **14**(1), 30–36 (2020).
2. K. C. Prince, E. Allaria, C. Callegari, R. Cucini, G. De Ninno, S. Di Mitri, B. Diviacco, E. Ferrari, P. Finetti, D. Gauthier, L. Giannessi, N. Mahne, G. Penco, O. Plekan, L. Raimondi, P. Rebernik, E. Roussel, C. Svetina, M. Trovò, M. Zangrando, M. Negro, P. Carpeggiani, M. Reduzzi, G. Sansone, A. N. Grum-Grzhimailo, E. V. Gryzlova, S. I. Strakhova, K. Bartschat, N. Douguet, J. Venzke, D. Iablonskiy, Y. Kumagai, T. Takanashi, K. Ueda, A. Fischer, M. Coreno, F. Stienkemeier, Y. Ovcharenko, T. Mazza, and M. Meyer, "Coherent control with a short-wavelength free-electron laser," *Nat. Photonics* **10**(3), 176–179 (2016).
3. V. Cardin, B. Schmidt, N. Thiré, S. Beaulieu, V. Wanie, M. Negro, C. Vozzi, V. Tosa, and F. Légaré, "Self-channelled high harmonic generation of water window soft x-rays," *J. Phys. B: At., Mol. Opt. Phys.* **51**(17), 174004 (2018).
4. T. Popmintchev, M.-C. Chen, D. Popmintchev, P. Arpin, S. Brown, S. Ališauskas, G. Andriukaitis, T. Balčiūnas, O. D. Mücke, A. Pugzlys, A. Baltuška, B. Shim, S. E. Schrauth, A. Gaeta, C. Hernández-García, L. Plaja, A. Becker, A. Jaron-Becker, M. M. Murnane, and H. C. Kapteyn, "Bright coherent ultrahigh harmonics in the keV x-ray regime from mid-infrared femtosecond lasers," *Science* **336**(6086), 1287–1291 (2012).
5. S. M. Teichmann, F. Silva, S. Cousin, M. Hemmer, and J. Biegert, "0.5-keV soft x-ray attosecond continua," *Nat. Commun.* **7**(1), 11493 (2016).
6. A. Cabasse, C. Hazera, L. Quintard, E. Cormier, S. Petit, and E. Constant, "Collection and spectral control of high-order harmonics generated with a 50 W high-repetition rate ytterbium femtosecond laser system," *J. Phys. B: At., Mol. Opt. Phys.* **49**(8), 085601 (2016).
7. H. Rubinsztein-Dunlop, A. Forbes, M. V. Berry, M. R. Dennis, D. L. Andrews, M. Mansuripur, C. Denz, C. Alpmann, P. Banzer, T. Bauer, E. Karimi, L. Marrucci, M. Padgett, M. Ritsch-Marte, N. M. Litchinitser, N. P. Bigelow, C. Rosales-Guzmán, A. Belmonte, J. P. Torres, T. W. Neely, M. Baker, R. Gordon, A. B. Stilgoe, J. Romero, A. G. White, R. Fickler, A. E. Willner, G. Xie, B. McMorrin, and A. M. Weiner, "Roadmap on structured light," *J. Opt.* **19**(1), 013001 (2017).
8. D. B. Milošević, W. Becker, and R. Kopold, "Generation of circularly polarized high-order harmonics by two-color coplanar field mixing," *Phys. Rev. A* **61**(6), 063403 (2000).
9. O. Kfir, E. Bordo, G. Ilan Haham, O. Lahav, A. Fleischer, and O. Cohen, "In-line production of a bi-circular field for generation of helically polarized high-order harmonics," *Appl. Phys. Lett.* **108**(21), 211106 (2016).
10. T. Fan, P. Grychtol, R. Knut, C. Hernández-García, D. D. Hickstein, D. Zusin, C. Gentry, F. J. Dollar, C. A. Mancuso, C. W. Hogle, O. Kfir, D. Legut, K. Carva, J. L. Ellis, K. M. Dorney, C. Chen, O. G. Shpyrko, E. E. Fullerton, O. Cohen, P. M. Oppeneer, D. B. Milošević, A. Becker, A. A. Jaroń-Becker, T. Popmintchev, M. M. Murnane, and H. C. Kapteyn, "Bright circularly polarized soft x-ray high harmonics for x-ray magnetic circular dichroism," *Proc. Natl. Acad. Sci.* **112**(46), 14206–14211 (2015).
11. O. Kfir, S. Zayko, C. Nolte, M. Sivils, M. Möller, B. Hebler, S. S. P. K. Arekapudi, D. Steil, S. Schäfer, M. Albrecht, O. Cohen, S. Mathias, and C. Ropers, "Nanoscale magnetic imaging using circularly polarized high-harmonic radiation," *Sci. Adv.* **3**(12), eaao4641 (2017).
12. M. Zürch, C. Kern, P. Hansinger, A. Dreischuh, and C. Spielmann, "Strong-field physics with singular light beams," *Nat. Phys.* **8**(10), 743–746 (2012).
13. G. Gariépy, J. Leach, K. T. Kim, T. J. Hammond, E. Frumker, R. W. Boyd, and P. B. Corkum, "Creating high-harmonic beams with controlled orbital angular momentum," *Phys. Rev. Lett.* **113**(15), 153901 (2014).
14. S. Ghimire, A. D. DiChiara, E. Sistrunk, P. Agostini, L. F. DiMauro, and D. A. Reis, "Observation of high-order harmonic generation in a bulk crystal," *Nat. Phys.* **7**(2), 138–141 (2011).
15. S. Ghimire and D. A. Reis, "High-harmonic generation from solids," *Nat. Phys.* **15**(1), 10–16 (2019).
16. M. Sivils, M. Taucer, G. Vampa, K. Johnston, A. Staudte, A. Y. Naumov, D. Villeneuve, C. Ropers, and P. Corkum, "Tailored semiconductors for high-harmonic optoelectronics," *Science* **357**(6348), 303–306 (2017).
17. D. Gauthier, S. Kaassamani, D. Franz, R. Nicolas, J.-T. Gomes, L. Lavoute, D. Gaponov, S. Fédrier, G. Jargot, M. Hanna, W. Boutou, and H. Merdji, "Orbital angular momentum from semiconductor high-order harmonics," *Opt. Lett.* **44**(3), 546–549 (2019).
18. S. Han, H. Kim, Y. W. Kim, Y.-J. Kim, S. Kim, I.-Y. Park, and S.-W. Kim, "High-harmonic generation by field enhanced femtosecond pulses in metal-sapphire nanostructure," *Nat. Commun.* **7**(1), 13105 (2016).

19. G. Vampa, B. Ghamsari, S. S. Mousavi, T. Hammond, A. Olivieri, E. Lisicka-Skrek, A. Y. Naumov, D. Villeneuve, A. Staudte, P. Berini, and P. B. Corkum, "Plasmon-enhanced high-harmonic generation from silicon," *Nat. Phys.* **13**(7), 659–662 (2017).
20. H. Liu, G. Vampa, J. L. Zhang, Y. Shi, S. Buddhiraju, S. Fan, J. Vuckovic, P. H. Bucksbaum, and D. A. Reis, "Beating absorption in solid-state high harmonics," *Commun. Phys.* **3**(1), 192 (2020).
21. H. Liu, C. Guo, G. Vampa, J. L. Zhang, T. Sarmiento, M. Xiao, P. H. Bucksbaum, J. Vučković, S. Fan, and D. A. Reis, "Enhanced high-harmonic generation from an all-dielectric metasurface," *Nat. Phys.* **14**(10), 1006–1010 (2018).
22. Y. S. You, D. A. Reis, and S. Ghimire, "Anisotropic high-harmonic generation in bulk crystals," *Nat. Phys.* **13**(4), 345–349 (2017).
23. S. Rashid, J. Walia, H. Northfield, C. Hahn, A. Olivieri, A. C. Lesina, F. Variola, A. Weck, L. Ramunno, and P. Berini, "Helium ion beam lithography and liftoff," *Nano Futures* (2021).
24. J. Liu, P. Jia, X. Chen, T. Liang, H. Liu, W. Liu, and J. Xiong, "Surface characterization of patterning on mgo single crystals using wet chemical etching process to advance mems devices," *J. Micromech. Microeng.* **30**(1), 015001 (2020).
25. A. Korobenko, T. Hammond, C. Zhang, A. Y. Naumov, D. Villeneuve, and P. Corkum, "High-harmonic generation in solids driven by counter-propagating pulses," *Opt. Express* **27**(22), 32630–32637 (2019).
26. G. Vampa, Y. You, H. Liu, S. Ghimire, and D. Reis, "Observation of backward high-harmonic emission from solids," *Opt. Express* **26**(9), 12210–12218 (2018).
27. S. H. Chew, K. Pearce, C. Späth, A. Guggenmos, J. Schmidt, F. Stüßmann, M. F. Kling, U. Kleineberg, E. Mårzell, C. L. Arnold, E. Lorek, P. Rudawski, C. Guo, M. Miranda, F. Ardana, J. Mauritsson, A. L'Huillier, and A. Mikkelsen, *Imaging Localized Surface Plasmons by Femtosecond to Attosecond Time-Resolved Photoelectron Emission Microscopy – ATTO-PEEM* (John Wiley and Sons, Ltd, 2014), chap. 10, pp. 325–364.
28. M. K. L. Man, J. Madéo, C. Sahoo, K. Xie, M. Campbell, V. Pareek, A. Karmakar, E. L. Wong, A. Al-Mahboob, N. S. Chan, D. R. Bacon, X. Zhu, M. M. M. Abdelrasoul, X. Li, T. F. Heinz, F. H. da Jornada, T. Cao, and K. M. Dani, "Experimental measurement of the intrinsic excitonic wave function," *Sci. Adv.* **7**(17), eabg0192 (2021).
29. M. X. Na, A. K. Mills, F. Boschini, M. Michiardi, B. Nosarzewski, R. P. Day, E. Razzoli, A. Sheyerman, M. Schneider, G. Levy, S. Zhdanovich, T. P. Devereaux, A. F. Kemper, D. J. Jones, and A. Damascelli, "Direct determination of mode-projected electron-phonon coupling in the time domain," *Science* **366**(6470), 1231–1236 (2019).
30. X. Yu, Q. Bian, B. Zhao, Z. Chang, P. Corkum, and S. Lei, "Near-infrared femtosecond laser machining initiated by ultraviolet multiphoton ionization," *Appl. Phys. Lett.* **102**(10), 101111 (2013).
31. X. Yu, Z. Chang, P. Corkum, and S. Lei, "Fabricating nanostructures on fused silica using femtosecond infrared pulses combined with sub-nanojoule ultraviolet pulses," *Opt. Lett.* **39**(19), 5638–5640 (2014).